CHAPTER 4

CHARACTERIZATION OF TM_{01} TO TE_{11} SWG MODE CONVERTER

*Part of this work has been published as:

Kumar V., Dwivedi S. and Jain P.K., "Mode Matching Analysis for Characterisation of the SWG Mode Converters," *Microwave and Optical Technology Letters*, 2019, v. 61, pp. 2619-2627.

SWG mode converters are realised with the coaxial waveguide structure separated by axially-radial metal plates. The mode conversion has been achieved through the length of the SWG region having two different sectoral angles [Kumar *et al.* (2019) and Yuan *et al.* (2005)]. Here, mode conversion analysis for TM_{01} modes to the TE_{11} mode using the coaxial waveguide and SWG sections need attention. In general waveguide filter, material characterization and bifurcation of power divider are analyzed using a faster and more precise technique mode matching [Andrade (2001), Huang and Zhang (2007), Hoppe (1988) and Matras (1996)]. So, to estimate the mode conversion due to waveguide discontinuity, the mode matching technique (MMT) proves to be an effective and useful method. In this technique, the step discontinuity arises between two waveguides junction is represented as the fundamental block through which other components, e.g., transitions, bifurcation, iris can be analysed [Arndt *et al.* (2005)]. Orfanidis *et al.* (2000) using the MMT for circular and coaxial waveguide discontinuities, where coupling coefficients for various modes are expressed. Mongiardo reported the concept of n-furcation of the elliptical waveguide [Mongiardo and Russer (1999)]. The conventional approach of finding modal scattering matrix, which has a subset of generalised scattering matrix (GSM), has been explained by Yang *et al.* (1993). Chang *et al.* have reported a mode-matching analysis of the SWGs [Chang *et al.* (1995)], where 12 metallic plates are inserted in a coaxial structure for the study a motor like structure, though this analysis limited to the reflected modes at sectoral apertures and applied to the radar cross-section measurements.

To the best of authors' knowledge mode-matching analysis for the SWG mode converter is not yet reported. In this Chapter, mode-matching analysis of coaxial waveguide to the trifurcated SWG is explored. Moreover, this present analysis also enables one the use of SWG in other applications as well. The S-band (3 GHz) SWG

mode converter design, simulation and experimental results reported in the previous Chapter of this thesis (Chapter 3). The mode matching analysis developed here is applied for further validation and evaluation of the performance of the developed mode converter reported in the previous Chapter.

4.1. Waveguide Theory

4.1.1 *TEM* mode in a coaxial waveguide

If the *TEM* mode is propagating the coaxial waveguide the field expressions are following

$$E_r = \eta \frac{I}{2\pi r} e^{-jk_0 z}, \tag{4.1a}$$

$$H_\theta = \frac{I}{2\pi r} e^{-jk_0 z}, \tag{4.1b}$$

where $\eta = (\mu_o / \varepsilon_o)^{1/2}$ [Montgomery (1948)].

4.1.2 *TE* modes in Cylindrical Coordinate System

Field analysis is undertaken to study the propagation time of the significant modes inside the chosen mode converter. The analysis requires the fields to be expressed regarding the solutions of the Helmholtz equation in the cylindrical coordinate system. These expressions are used to establish the structure-parameter relation with the phase propagation constant and obtain the scattering coefficients of the mode converter for the desired and closely related modes [Balanis (1989), Harrington (2001) and Basu (2015)]. In the present case, the chosen structure of the mode converter is a combination of a coaxial waveguide and several SWGs. An SWG consists of a sector formed by partitioning a coaxial waveguide with conducting plates (as discussed in Section 1.4). In the SWG mode converter, mode conversion depends upon the sectoral angle and sectoral plate length (as discussed in Sections 1.4 and 3.1).

The scalar Helmholtz equation $(\nabla^2 H_z + k_0^2 H_z = 0)$ is applicable for *TE* modes, where k_0 is the free-space propagation constant. The method of separation of variables requires the expression $H_z\{r,\theta,z\} = R\{r\}P\{\theta\}\mathbb{Z}\{z\}$, where $R\{r\}$, $P\{\theta\}$ and $\mathbb{Z}\{z\}$ are functions of the radial, azimuthal and axial coordinates, respectively. Now, substituting $H_z\{r,\theta,z\}$ in its separable form into the wave equation results in the following:

$$\frac{1}{R\{r\}}\left(\frac{d^2R\{r\}}{dr^2}+\frac{1}{r}\frac{dR\{r\}}{dr}\right)+\frac{1}{P\{\theta\}}\frac{1}{r^2}\frac{d^2P\{\theta\}}{d\theta^2}+\frac{1}{\mathbb{Z}\{z\}}\frac{d^2\mathbb{Z}\{z\}}{dz^2}+k_0^2=0 \quad . \qquad (4.2)$$

Solution of (4.1) is given by:

$$H_z\{r,\theta,z\} = \left(A^{(1)}J_m\{\gamma r\}+B^{(1)}Y_m\{\gamma r\}\right)\left(A^{(2)}\cos\{m\theta\}+B^{(2)}\sin\{m\theta\}\right) \times\left(A^{(3)}e^{j\beta z}+B^{(3)}e^{-j\beta z}\right) \quad , (4.3)$$

where J_m and Y_m are the Bessel functions of first and second kind of the order *m*; $A^{(1)}, B^{(1)}, A^{(2)}, B^{(2)}, A^{(3)},$ and $B^{(3)}$ are field constants. Here, $m(=-\sqrt{\partial^2/\partial\theta^2})$ being the azimuthal constant express the half period azimuthal variation number and $\gamma(=[k_0^2-\beta^2]^{1/2})$ is the radial propagation constant regarding the axial propagation constant β, and free-space propagation constant k_0. By virtue of the principle of superposition, the general solution is:

$$H_z\{r,\theta,z\} = \sum_{m=1}^{\infty}\left[\left(A_m^{(1)}J_m\{\gamma r\}+B_m^{(1)}Y_m\{\gamma r\}\right) \times\left(A_m^{(2)}\cos\{m\theta\}+B_m^{(2)}\sin\{m\theta\}\right)\left(A_m^{(3)}e^{j\beta z}+B_m^{(3)}e^{-j\beta z}\right)\right] \quad . \qquad (4.4)$$

Leading to

$$E_\theta\{r,\theta,z\} = \sum_{m=1}^{\infty}E_{\theta,m}\{r,\theta,z\} = j\frac{\omega\mu}{\gamma}\sum_{m=1}^{\infty}\left[\left(A_m^{(1)}J'_m\{\gamma r\}+B_m^{(1)}Y'_m\{\gamma r\}\right) \times\left(A_m^{(2)}\cos\{m\theta\}+B_m^{(2)}\sin\{m\theta\}\right)\left(A_m^{(3)}e^{j\beta z}+B_m^{(3)}e^{-j\beta z}\right)\right] \quad , \qquad (4.5)$$

where $A_m^{(1)}, B_m^{(1)}, A_m^{(2)}, B_m^{(2)}, A_m^{(3)}, \text{and } B_m^{(3)}$ are field constants in which some are found using boundary conditions. Also, J'_m and Y'_m are the derivatives of first and second kinds of the Bessel function.

4.1.2.1 Coaxial waveguide

A coaxial waveguide is made up of two concentric conducting cylinders, with the space between two acting as a waveguide. Let the radius of the inner cylinder be r_i and the radius of the outer cylinder as r_o. $A_m^{(3)} \equiv 0$ for the forward wave propagation. Next, $A_m^{(1)} J'_m\{\gamma r_i\} + B_m^{(1)} Y'_m\{\gamma r_i\} = 0$ because $E_\theta\{r,\theta,z\}\big| = 0$ at, the inner radius of the coaxial waveguide. Hence:

$$H_z = \sum_{m=1}^{\infty} H_{z,m} = \sum_{m=1}^{\infty} T_m \; X_m\{\gamma r\}[A_m^{(2)} \cos\{m\theta\} + B_m^{(2)} \sin\{m\theta\}]\, e^{-j\beta z} \quad , \tag{4.6}$$

and

$$E_\theta = \sum_{m=1}^{\infty} E_{\theta,m} = j\frac{\omega\mu}{\gamma} \sum_{m=1}^{\infty} T_m \; X'_m\{\gamma r\}[A_m^{(2)} \cos\{m\theta\} + B_m^{(2)} \sin\{m\theta\}]\, e^{-j\beta z} \quad . \tag{4.7}$$

Furthermore,

$$E_r = -j\frac{\omega\mu m}{r\gamma^2} \sum_{m=1}^{\infty} T_m \; X_m\{\gamma r\}[B_m^{(2)} \cos\{m\theta\} - A_m^{(2)} \sin\{m\theta\}]\, e^{-j\beta z} \tag{4.8}$$

where T_m is a product of constants as:

$$T_m = A_m^{(1)} B_m^{(3)} \tag{4.9}$$

moreover, $$X_m\{\gamma r\} = J_m\{\gamma r\} \; Y'_m\{\gamma r_i\} - J'_m\{\gamma r_i\} Y_m\{\gamma r\} \quad , \tag{4.10}$$

and $$X'_m\{\gamma r\} = J'_m\{\gamma r\}\ Y'_m\{\gamma\, r_i\} - J'_m\{\gamma\, r_i\} Y'_m\{\gamma r\}\,. \tag{4.11}$$

Now, using boundary condition at the outer metallic cylindrical surface of the coaxial waveguide, $E_\theta\{r,\theta,z\}\big| = 0$ at $r = r_o$; hence,

$$\sum_{m=1}^{\infty} T_m\, X'_m\{\gamma r_o\} = 0\,. \tag{4.12}$$

Thus, the dispersion relation of the coaxial guide becomes:

$$X'_m\{\gamma r_o\} = 0\ . \tag{4.13}$$

The roots of (4.13) are labelled n = 1, 2, 3, … and the mocks as TE_{mn}. Other than the *TEM* mode, the lowest mode is TE_{11}. In the remainder of this paper, only TE_{m1} modes are considered.

4.1.2.2 Sectoral Waveguide (SWG)

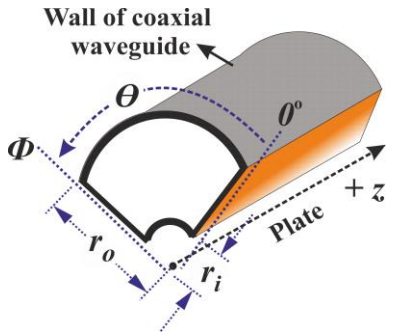

Figure 4.1. The typical structure of the sectoral waveguide (SWG).

The separation of the coaxial waveguide in some angular sectors by inserting conducting plates in the axial-radial direction yields some sectoral waveguide (SWG). The SWG is found handy to obtain desired mode conversion in the HPM system [Yuan *et al*. (2005)]. In the SWG integer p denotes the number of half period variation as SWG model field [Elsherbeni *et al*. (1991)]. The constant $B^{(2)} = 0$ because $E_r\{r,\theta,z\}\big| = 0$ at $\theta = 0°$, the right side wall of the SWG. Next, $\sin\{m\phi\} = 0$ because $E_r\{r,\theta,z\}\big| = 0$ at $\theta = \phi$, left side wall of the SWG, so that $m\phi = p\pi$. Here it is noticeable that subscript m of the

coaxial waveguide is replaced by p as a value of modal order, while in equations constant m is replaced by $p\pi/\phi$. Hence

$$E_r = \sum_{p=1}^{\infty} E_{r,p} = -j\frac{\omega\mu(p\pi/\phi)}{r\gamma^2}\sum_{p=1}^{\infty} T_p\, W_p\{\gamma r\}\sin\{(p\pi/\phi)\theta\}\, e^{-j\beta z} \tag{4.14}$$

$$H_z = \sum_{p=1}^{\infty} H_{z,p} = \sum_{p=1}^{\infty} T_p\, W_p\{\gamma r\}\cos\{(p\pi/\phi)\theta\}\, e^{-j\beta z} \tag{4.15}$$

$$E_\theta = \sum_{p=1}^{\infty} E_{\theta,p} = j\frac{\omega\mu}{\gamma}\sum_{p=1}^{\infty}\gamma T_p\, \mathrm{W}'_p\{\gamma\,\mathrm{r}\}\cos\{(p\pi/\phi)\theta\}\; e^{-j\beta z} \quad , \tag{4.16}$$

where T_p is the product of constants as:

$$T_p = A_p^{(1)}\, A_p^{(2)}\, B_p^{(3)} \tag{4.17}$$

moreover, $$W_p\{\gamma r\} = J_{(p\pi/\phi)}\{\gamma r\}\; Y'_{(p\pi/\phi)}\{\gamma\, r_i\} - J'_{(p\pi/\phi)}\{\gamma\, r_i\}Y_{(p\pi/\phi)}\{\gamma r\}\,, \tag{4.18}$$

$$W'_p\{\gamma r\} = J'_{(p\pi/\phi)}\{\gamma r\}\; Y'_{(p\pi/\phi)}\{\gamma\, r_i\} - J'_{(p\pi/\phi)}\{\gamma\, r_i\}Y'_{(p\pi/\phi)}\{\gamma r\}\,. \tag{4.19}$$

Now, using boundary condition at the outer metallic surface of the SWG, $E_\theta\{r,\theta,z\}\big| = 0$ at $r = r_o$; hence,

$$\sum_{p=1}^{\infty} T_p\, W'_p\{\gamma r_o\} = 0\,. \tag{4.20}$$

Thus, the dispersion relation of the sectoral waveguide (SWG) becomes:

$$W'_p\{\gamma r_o\} = 0\ . \tag{4.21}$$

The roots of (4.21) are labelled n = 1, 2, 3, … and the mocks as TE_{pn}. The dominant mode is TE_{11}. In the remainder of this paper, only TE_{p1} modes are considered.

4.2. Mode-Matching Technique (MMT)

Mode-matching technique (MMT) is one of the accurate methods to study waveguide discontinuities. It is now becoming a standard approach for characterization of waveguide transformers, filters, multiplexers, polarizers, or mode converter transducers.

The amplitude of each mode affects the excitation of modes in the adjacent region or sub-region and their boundary conditions. This shows the importance of MMT, unlike other numerical methods, MMT reduces the EM problem to a linear system based on the amplitude of each mode (scalar complex numbers) in each regions and subregions, rather than the vector fields at each point of a 3D electromagnetic simulation. This provides an opportunity of reduction in simulation time by eliminating the number of junk unknowns; as well as a more faithful representation of the EM fields, which leads to both a fast and precise resolution of the EM problem. The model designed in Chapter 3, as shown in Figure 4.2, is characterized in this Chapter using MMT.

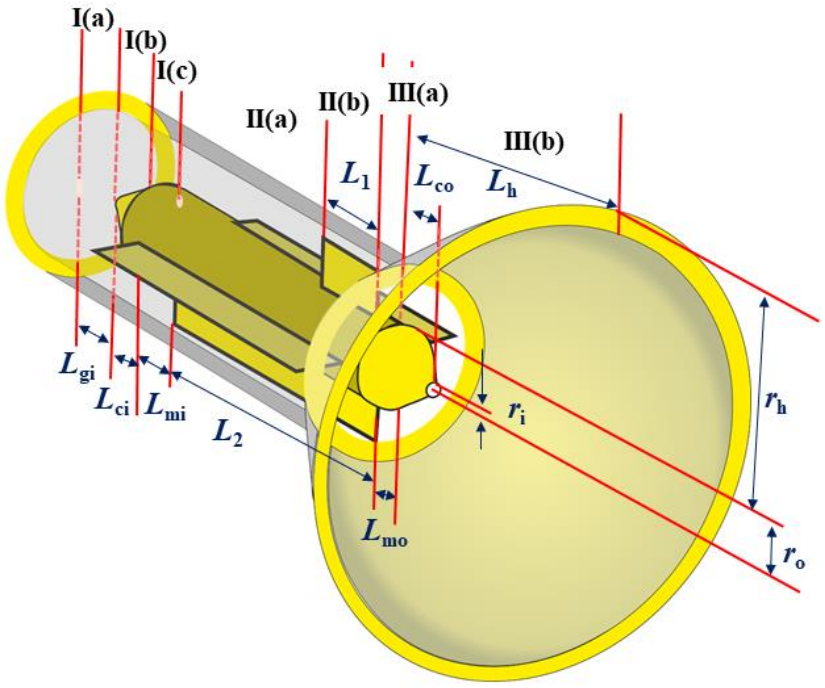

Figure 4.2. The typical model of TM_{01} to TE_{11} SWG mode converter with a conical horn antenna.

4.2.1 Theory of Characterization of SWG Mode Converters:

While reviewing the different techniques used for the characterization of SWG mode converters reported in the literature. The dispersion relation of sectoral waveguide was expressed by Lin *et al*. 1989. The mode matching analysis of SWG, as metallic blades in a cylinder, to analyse the effects of radiation on fighter aircraft wing has reported by Mongiardo and Russer (1999). Also, a junction of four ridged-SWG to ridged-coaxial waveguide designed, their experimental results have been reported by Zang *et al*. (2002). First reported SWG mode converter has simulated and validated with their experimental results by Yuan *et al*. 2005. Similarly, the SWG mode converters reported using dielectric material to help mode conversion and the results are validated using experimental measurements [Chittora *et al.* (2015)]. Integral equation and Galerkin's Method of Moment are used for analysis SWG Arrays with multi-layered radomes [Kalfa *et al*. (2016)]. Till now the mode-matching analysis of SWG mode converter is not available in the published literature.

Mode matching analysis is done to determine the scattering coefficients for all the modes excited in the system. In this analysis, the structure is segmented at each discontinuity. The boundary conditions at the plane of discontinuities for the tangential electric and magnetic fields, regarding their corresponding modes, are applied. The power of electromagnetic waves in each region is weighted by utilization of the orthogonal properties of the waveguide modes, and the corresponding coupling coefficients are also thus obtained [Klaren (1994)].

The MMT is a rigorous analytical technique uses the coupling coefficient and wave impedances to determine the scattering coefficients. Since the amplitudes of higher-order modes fall off rapidly, so it is reasonable to truncate such waveguide modes to a finite number of terms, as a fair approximation [Klaren (1994)]. So, this is an

accurate and faster technique in determining the modal powers at the disturbance in the waveguide or its junctions.

A typical model of TM_{01} to TE_{11} SWG mode converter is shown in Figure 4.2, where waveguide sections of the converter structure at its discontinuity are divided into distinct regions in the axial length. Region *II* refer to the sections where axially radial metal plates divide the coaxial waveguide into three SWGs shown in Figure 4.2. Here, at the input end of the converter, between the circular waveguide and coaxial guide a tapered coaxial section of approximately $\lambda/2$ lengths are used for impedance matching, and ~ 99.9% mode conversion has thus achieved. Further, Region *II*, SWG_{π} is divided into two $SWG_{\pi/2}$ sections. The MMT has adapted for the ports D to F, and the typical model is shown in Figure 4.3.

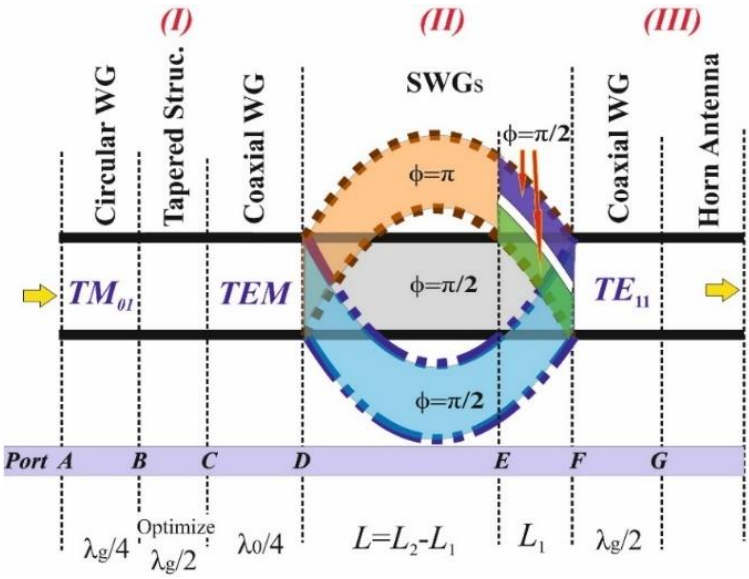

Figure 4.3. A typical model of TM_{01} to TE_{11} SWG mode converter along their axial length.

For obtaining the scattering coefficients of the mode converter, mode-matching method is used, which requires knowledge of electric and magnetic fields components for the relevant mode in the different regions and sub-regions of the SWG mode converter. Using the time average of Poynting vector the field amplitudes are

normalized. The normalized field functions are used to determine the coupling coefficients for different modes that are coupling at the different junction and is described in detail in the section 4.2.3. The coupling coefficient between modes in different regions at a junction and the wave impedances of the concerned regions are used to obtain the elements of generalized scattering matrix (GSM) of the junction. Combining all GSM conclude to the scattering matrix of the complete structure [Arndt *et al*. (2005)].

4.2.2 Evaluation of the Field Constants

For evaluation of the field constants occurring in the field equations (4.1) and (4.3 to 4.8), it is required to normalize them, so that the power carried in each mode is become unity for the propagating modes and becomes independent of the magnitude of excitation [Arndt *et al*. (2005), Orfanidis *et al*. (2000), Li (2014) and Klaren (1994)]. Applying the time average of Poynting vector equal to unity, the product of field constants I, T_{m}, and T_{p} are measured as following

$$\left|\frac{1}{2}\int_{s}\vec{E}\times\vec{H}^{*}.\mathrm{ds}\right|=1. \tag{4.22}$$

For the coaxial waveguide *TEM* mode by substituting (4.1) in (4.22), the electric and magnetic fields are multiplied and integrated over the radial-azimuthal plane. This results in the expression for field constant of equation (4.1) as following

$$I=\left(\frac{4\pi}{\eta\, ln(r_o/r_i)}\right)^{1/2}. \tag{4.23}$$

The field constant of the coaxial waveguide for TE_{m1} mode expressed in (4.3) has chosen for a particular mode (depends upon m). By substituting (4.3) in (4.5) the electric and magnetic field expressions are cross multiplied and integrated over the

radial-azimuthal plane. So, the expression for field constant of equation (4.3) is obtained as following

$$T_m = \gamma_{coax} \Bigg/ \left(2\pi\omega\mu_o\beta_{coax} \bullet \int_{r_i}^{r_o} \begin{pmatrix} rX'^2\{\gamma_{coax}^2 r\} + \\ (m^2/\gamma_{coax}^2 r)X'^2\{\gamma_{coax}^2 r\} \end{pmatrix} dr \right)^{1/2}, \qquad (4.24)$$

where, γ_{coax} is radial propagation constant and β_{coax} axial propagation constant of the coaxial waveguide. Similarly, the field constant of the SWG for TE_{p1} mode expressed in (4.4) is chosen for a particular mode (depends upon *p*). Again, substituting (4.4) in (4.5) electric and magnetic fields are cross-multiplied and integrated over the radial-azimuthal plane of SWG cross-section and yields

$$T_p = 2\gamma_{SWG} \Bigg/ \left(\omega\mu_o\beta_{SWG}\phi \bullet \int_{r_i}^{r_o} \begin{pmatrix} rW'^2\{\gamma_{SWG} r\} + \\ (m^2/\gamma_{SWG}^2 r)W'^2\{\gamma_{SWG} r\} \end{pmatrix} dr \right)^{1/2}, \qquad (4.25)$$

where γ_{SWG} is radial propagation constant of SWG. All the field constants normalized by substituting (4.26), (4.27) and (4.28) in their relevant field expressions, for further calculation. To account for all possible modes, the orthogonal relations are applied to find the scattering coefficients at the junctions. These scattering coefficients constitute the generalized scattering matrix (GSM) for a junction.

4.2.3 Coupling Coefficient

The coupling coefficients can be obtained by equating the tangential electric and magnetic fields at the junction, multiplying by orthogonal fields and integrating over the boundary values [Arndt *et al*. (2005), Orfanidis *et al*. (2000), Li (2014) and Klaren (1994)]. Using field equations (4.1), (4.3) - (4.8) and field constants (4.23) - (4.25), normalized coupling coefficients are obtained and expressed. Since MMT is applied only on the junction of abrupt discontinuity, so the coupling of modes between port-D, port-E, and port-F are taken into account. To measure all possible modes at such ports,

the following orthogonality relations applied, which provides the coupling coefficient as following

$$C_{ij} = \iint_s (\bar{H}^i \times \bar{E}^j) \bullet \bar{z}\, ds \tag{4.26}$$

where $\bar{z}$ is the unit vector in the direction of propagation. Here C_{ij} is the coupling coefficient at any junction, where mode *i* in one region is coupled to mode *j* in the second region. The coupling coefficient for the interface of the coaxial waveguide and the SWG is as following

$$C_p = \iint_s (\bar{H}_\theta^{TEM} \times \bar{E}_r^{TE(p)}) \bullet \bar{z}\, ds \tag{4.27}$$

where *s* denotes, the cross-section of SWG and *p* denotes the order of modes in them. The coupling coefficient between *TEM* to TE_{p1} mode can express as follows

$$C_p = -IT_p\, j \frac{\omega\mu}{2\pi\gamma_{SWG}^2} \left[\int_{r=r_i}^{r_o} \frac{W_o\{\gamma r\}}{r}\, dr \right] \left[\int_{\theta=0}^{\phi} (p\pi/\phi) \sin\{(p\pi/\phi)\theta\} d\theta \right]. \tag{4.28}$$

Similarly, at the junction of SWG_{π} and $SWG_{\pi/2}$ the coupling coefficient will be following

$$C_{p_{(\pi)} p_{(\pi/2)}} = \iint_s (\bar{E}_r^{TE(p_{(\pi)})} \times \bar{H}_\theta^{TE(p_{(\pi/2)})}) \bullet \bar{z}\, ds \tag{4.29}$$

where *s* denotes, the cross-section of $SWG_{\pi/2}$ and $p(\pi)$ and $p(\pi/2)$ denotes the order of modes in SWG_{π} and $SWG_{\pi/2}$, respectively. The coupling coefficient between TE_{p1} modes of the SWG_{π} to TE_{p1} modes of the $SWG_{\pi/2}$ can express as:

$$C_{p_{(\pi)} p_{(\pi/2)}} = -T_{p_{(\pi)}} \times T_{p_{(\pi/2)}} \times \frac{\omega\mu\, \beta_{(\pi/2)}}{\gamma_{(\pi)}\, \gamma_{(\pi/2)}} \left(\begin{array}{l} \int_{r=r_i}^{r_o} W'_{o(\pi)}\{\gamma r\} W'_{o(\pi/2)}\{\gamma r\}\, r\, dr \cdot \int_{\theta=0}^{\phi} \cos\{p_{(\pi)}\theta\} \cos\{2p_{(\pi/2)}\theta\} d\theta \\ + \dfrac{1}{\gamma_{(\pi)}\, \gamma_{(\pi/2)}} \int_{r=r_i}^{r_o} \dfrac{1}{r} W_{o(\pi)}\{\gamma r\} W_{o(\pi/2)}\{\gamma r\}\, dr . \int_{\theta=0}^{\phi} \sin\{p_{(\pi)}\theta\} \sin\{2p_{(\pi/2)}\theta\} d\theta \end{array} \right), \tag{4.30}$$

where $T_{P(\pi)}$ and $T_{P(\pi/2)}$ are the field constants in $SWG\pi$ and $SWG_{\pi/2}$, respectively. Here the radial propagation constant γ_{coax} and axial propagation constant β_{coax} is for coaxial

waveguide relevant mode, also radial propagation constant γ_{SWG} for SWG relevant mode. At the junction of $SWG_{\pi/2}$ and coaxial waveguide the coupling coefficient will become:

$$C_{pm} = \iint_{s} (\bar{E}_r^{TE(p)} \times \bar{H}_\theta^{TE(m)}) \bullet \bar{z}\, ds\,. \tag{4.31}$$

The coupling coefficient between TE_{p1} modes of the SWG to TE_{m1} modes of the coaxial waveguide can be expressed as:

$$C_{pm} = T_p \times T_m \times j \frac{\omega\mu\, \beta_{coax}}{\gamma_{(\pi/2)}\, \gamma_{coax}} \left(\begin{array}{l} +\int_{r=r_i}^{r_o} X_o'\{\gamma r\} W_{o(\pi/2)}'\{\gamma r\}\, r\, dr \bullet \int_{\theta=0}^{\phi} \left(\cos\{2p_{(\pi/2)}\theta\} (\cos\{m\theta\} + \sin\{m\theta\}) \right) d\theta \\ -\frac{1}{\gamma_{(\pi/2)}\gamma_{coax}} \int_{r=r_i}^{r_o} \frac{1}{r} X_o\{\gamma r\} W_{o(\pi/2)}\{\gamma r\}\ dr \bullet \int_{\theta=0}^{\phi} \left(\begin{array}{l} 2p_{(\pi/2)} \sin\{2p_{(\pi/2)}\theta\} \bullet \\ m(\cos\{m\theta\} - \sin\{m\theta\}) \end{array} \right) d\theta \end{array} \right) \tag{4.32}$$

With this procedure, coupling coefficients (4.28), (4.30), and (4.32) are computed and are used in obtaining GSM discussed in Section 4b.

4.2.4 Generalized Scattering Matrix (GSM)

The total amplitude of EM fields may express in summation form of forwarding and backward travelling waves. So, equations for electric fields and magnetic fields in region-(u) can be written regarding potential and current form as following

and

$$\begin{aligned} V^{(u)}\{r,\theta\} &= \sum_{q=1} (a_q + b_q) (\sqrt{Z_c^{(u)}})_q \\ I^{(u)}\{r,\theta\} &= \sum_{q=1} (a_q - b_q) (\sqrt{Z_c^{(u)}})_q^{-1} \end{aligned} \tag{4.33}$$

where q denotes the number of modes in the region. The proposed SWG mode converter design has three abrupt discontinuities at port-D, port-E, and port-F. At any junction, the coupling between modes i to j from one region to another region, with the potential and current are expressed as follows

and

$$V_i^{(1)}\{r,\theta\} = V_j^{(2)}\{r,\theta\} C_{ij}\{r,\theta\}$$
$$I_j^{(2)}\{r,\theta\} = -I_i^{(1)}\{r,\theta\}\, C_{ij}\{r,\theta\} \quad , \tag{4.34}$$

where $C_{ij}\{r,\theta\}$ is the coupling coefficient at a junction between different modes. Multiplying the coupling coefficients with wave impedance of different modes coupling at the junction provides the row matrix as follows [Mongiardo and Russer (1999)]:

$$[Q]_{ij} = \left[\sqrt{Z_i}\right]^{-1} [C]_{ij} \left[\sqrt{Z_j}\right] \quad , \tag{4.35}.$$

where suffix i and j denote modes of two regions creating a junction. The Z_i and Z_j denote the modal impedances, which can be obtained by cut off frequency as according to Table 4.1. Also, the element of $[Q]_{ij}$ is known as coupling integrals, and the row matrix $[C]_{ij}$ is known as coupling integral and comprises of all the coupling coefficients between possible modes $\left([C]_{ij} = [C_{11}, C_{12}, .., C_{21}, C_{22}, ...C_{ij}]\right)$. This row matrix is used in evaluating *S*-parameter due to discontinuity at the junction.

Table 4.1. The cut-off frequency in GHz, at the different SWG for different modes.

Waveguide	*TEM*	TE_{11}	TE_{21}	TE_{31}
Coaxial	0	1.108	2.197	3.252
SWG_{π}	--	1.108	2.197	3.252
$SWG_{\pi/2}$	--	2.197	4.266	6.973

By solving the above equation following sets of the scattering matrix parameter are obtained as:

$$[S_{11}]_{mp}\Big|_{\phi} = \left([Q]_{mp}[Q]'_{mp} + [I]\right)^{-1}\left([Q]_{mp}[Q]'_{mp} - [I]\right) \tag{4.36a}$$

$$[S_{12}]_{mp}\Big|_{\phi} = 2\left([Q]_{mp}[Q]'_{mp} + [I]\right)^{-1}[Q]_{mp} \tag{4.36b}$$

$$[S_{21}]_{mp}\Big|_{\phi} = 2\left([Q]'_{mp}[Q]_{mp} + [I]\right)^{-1}[Q]'_{mp} \tag{4.36c}$$

$$[S_{22}]_{mp}\Big|_{\phi} = -\left([Q]'_{mp}[Q]_{mp} + [I]\right)^{-1}\left([Q]'_{mp}[Q]_{mp} - [I]\right) \tag{4.36d}$$

The above expressions are used in defining computational codes of mode matching analysis, where *m* signifies relevant modes in coaxial waveguide and *p* signifies the relevant modes in SWG. The analysis is performed for discontinuity of coaxial waveguide to SWGs, SWG to SWGs and SWG to the coaxial waveguide. Using expressions (4.36), the information about the possible modes present in the SWG mode converter could be determined in terms of the scattering coefficients.

4.3.Results and Discussion

The mode matching technique (MMT) used here for the prediction of the specific modes present at the output port of the design reported is first verified for a step discontinuity. In order to perform such verification, a junction between coaxial to SWG has been considered as well. The two junctions are coaxial to SWG_{π} and coaxial to $SWG_{\pi/2}$ apparent in the inset of Figures 4.4 and 4.5. It can easily be seen from these figures that the simulated and analytical values of scattering coefficients S_{11} and S_{21} for both the transitions are in the close agreement.

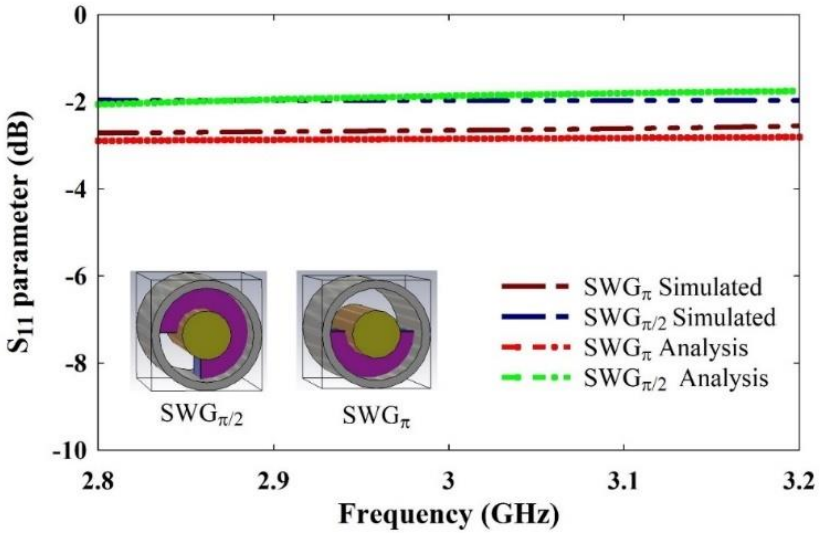

Figure 4.4. Return loss for a coaxial waveguide to SWG_{π} and a coaxial waveguide to $SWG_{\pi/2}$ transitions. The continuous coaxial waveguide has been blocked by sectoral conducting block, and the remaining unblocked path provides an abrupt change in the coaxial aperture to SWG aperture. The input port is on the coaxial waveguide side where return loss has obtained.

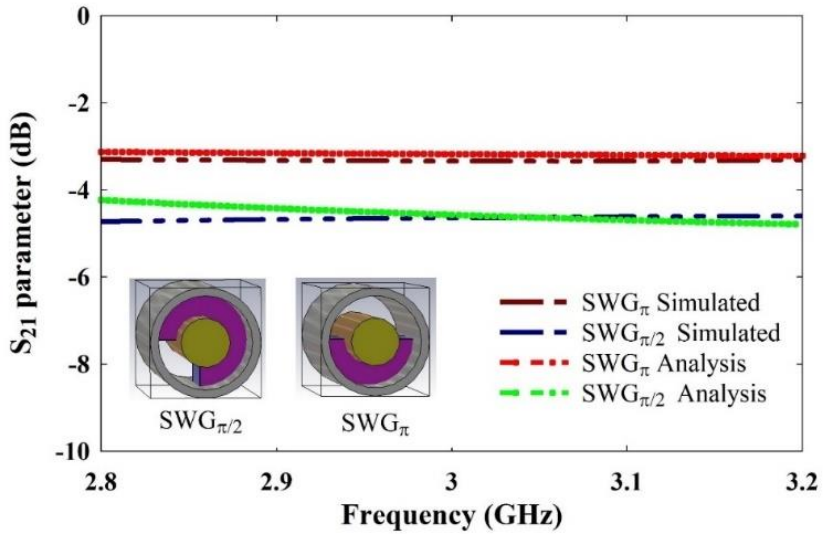

Figure 4.5. Transmission loss for a coaxial waveguide to SWG_{π} and a coaxial waveguide to $SWG_{\pi/2}$ transitions. The input port is on the coaxial waveguide side and output port is on the SWG side.

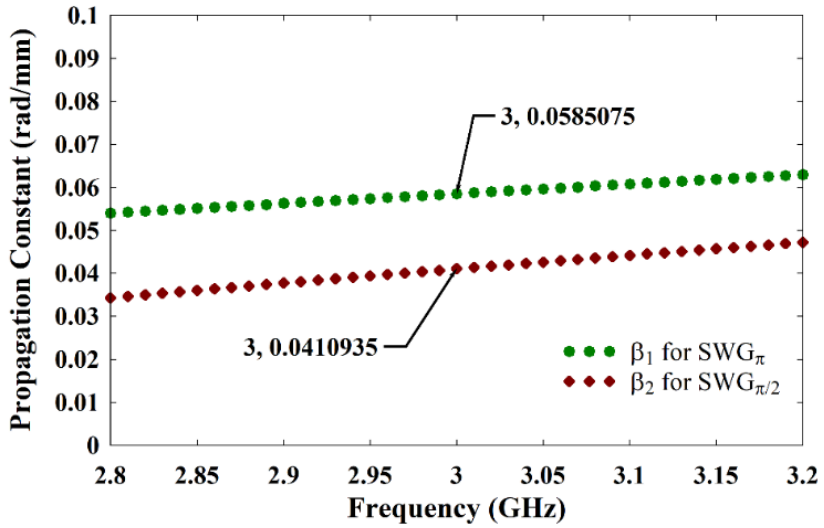

Figure 4.6. The propagation constant of SWG_{π} and $SWG_{\pi/2}$ according to variation in frequency.

Figure 4.6 shows the plots of the propagation constant versus the operating frequency for the SWG_{π} and $SWG_{\pi/2}$, and the separation between the two SWG's are due to the difference in its radial-azimuthal cross-sectional size. At 3 GHz frequency, length of Region II(a): $(L_2 - L_1 = \pi/(\beta_1 - \beta_2))$, required to set the orientation of field lines in the same direction approximately equals to 180 mm. In order to predict the different

modes, present at the output of this structure, one can take resort of the matching technique for the SWG mode converter from port-C to port-G.

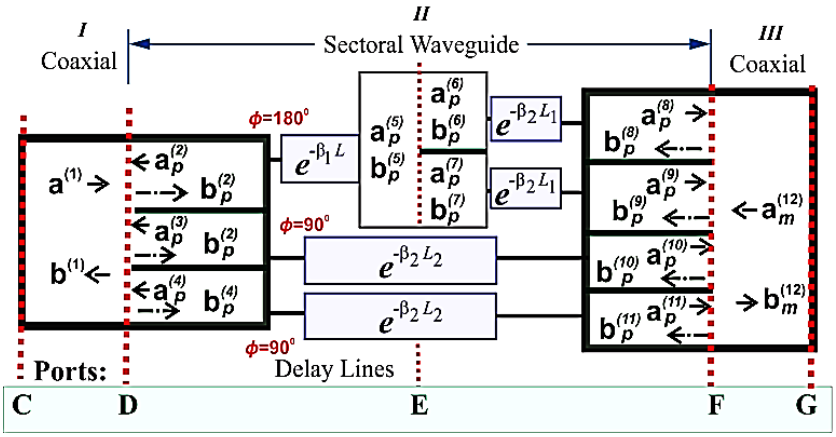

Figure 4.7. Scheme of the forward and backward wave at the different ports for the MMT. Fix delay length SWGs is cascaded with SWGs.

Using different junctions, a diagram of sub-regions of SWG mode converter in order to perform the mode matching analysis is shown in Figure 4.6. The MMT applied to the junction of port-D, port-E, and port-F. Also delay lines are provided in Figure 4.7, to measures the phase delay occurring due to propagation through different SWGs. For the port-D GSM1, port-E GSM2 and for port-F GSM3 are calculated. The three SWGs of Region *II*(a), scattering parameters in GSM1 are treated with delay lines. To enhance the processing time and avoiding complexity due to the delay line, the characteristic impedance has replaced by input impedance using the transformation of impedance [Montgomery (1948)]. At the port-E, SWG_{π} is bifurcated in two $SWG_{\pi/2}$ using *Plate1*, so the GSM2 has calculated. At the port-F GSM3 has calculated, where all the four $SWG_{\pi/2}$ are combined in one coaxial waveguide. The GSMs are of different sizes, so the complete structure GSM is obtained by manual calculation due to mismatch of matrix size.

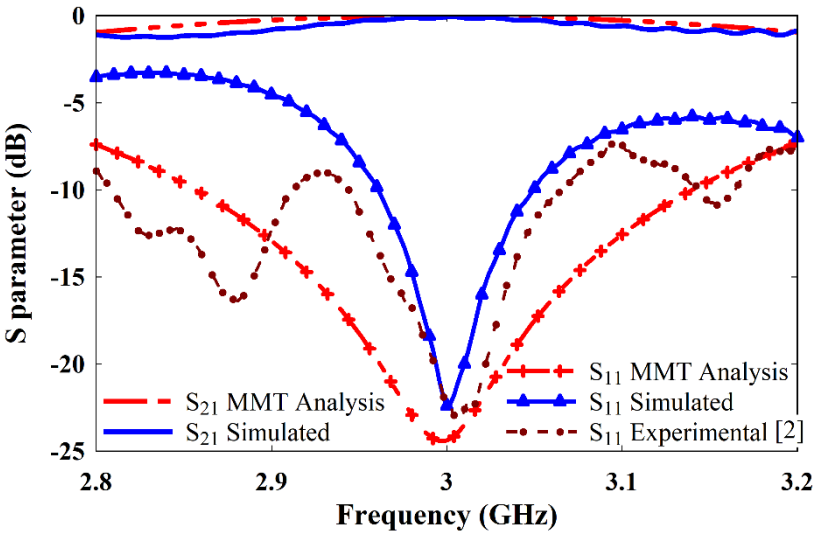

Figure 4.8. Transmission loss obtained from simulation between the input port-A to output port-G has been compared with the result obtained from the analysis using input port-C to output port-G. Also, the reflection loss obtained from the simulation at the port-A has been compared with the result obtained from analysis at the input port-C and with the measured value obtained at the input end [Kumar *et al*. (2019)].

The scattering coefficients S_{11} and S_{21} for different values of the operating frequency for this SWG mode converter structure is computed using the expression (4.12) developed in the previous section and simulated using commercial code CST Microwave Studio. The S_{11} using mode-matching method is -24.38 dB. It is plotted as Figure 4.8, where it could be appreciated that the developed analytical results for the power transmitted through the mode converter and power reflected at the input port are good in agreement with those obtained through simulation and experimental results [Kumar *et al*. (2019)]. The MMT is better in predicting mode generated at the abrupt junction, and it reveals the generation of TE_{21} mode at the port-F by all $SWG_{\pi/2}$. But due to orthogonal polarisation, mode combining of TE_{21} mode from all four $SWG_{\pi/2}$ results in TE_{11} mode over the coaxial waveguide, and this phenomenon reported in [Kumar *et al*. (2019)]. So, for the simplification in computational analysis, it is desirable to keep *Plate1* at the end of port-F. CST Microwave Studio works on FIT (Finite Integration Technique) which helps in analysing results of mode combining at end of trifurcation

of the coaxial waveguide. The gap between the curve of analytical and simulated results shows the characteristic of the different measurement technique.

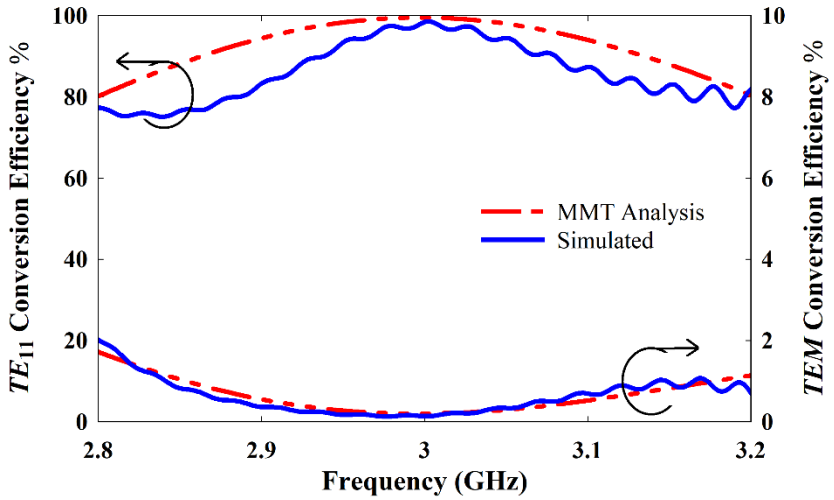

Figure 4.9. Comparison of conversion efficiency obtained from simulation between the input port-A to output port-G are compared with results obtained from the MMT analysis using input port-C to output port-G.

The SWG mode converter performance depends upon the conversion efficiency, and it is shown in Figure 4.8. For the frequency range of 2.8 GHz to 3.2 GHz, the conversion efficiency of the SWG mode converter is obtained. For TE_{11} mode conversion efficiency using mode-matching method is 99.14% and by the simulation is 98.62%. Also, for *TEM* at the output port, the mode conversion efficiency using mode-matching method is 0.32% and by the simulation is 0.18%. Again, the comparison shows good agreement between mode-matching analysis and simulation results with mode conversion efficiency higher than ~98.0% at 3 GHz. Other higher-order modes do not evolve at the port-F except TE_{21} mode, whereas this mode is forced to convert into lower-order mode TE_{11} or *TEM* due to the orthogonal orientation of all four $SWG_{\pi/2}$ [Kumar *et al*. (2019)]. Approximate computation time taken by mode-matching analysis is 11 minutes and simulation time taken by CST Microwave Studio is 50 minutes with 15 cells per wavelength near to model. So, it concludes that the MMT reported here is very efficient in computing the *S*-parameters and conversion efficiency.

Table 4.2: Comparison modal power distribution in SWG mode converter having *Plate1 and* without *Plate1*.

Power of Output Mode	Mode Converter with *Plate1*	Mode Converter without *Plate1*
TEM	0.32%	0.54%
TE_{11}	99.14%	91.87%
TE_{21}	0%	6.28%
TE_{31}	0%	0%

The modal power calculation has been obtained by the analysis. It is considered that the power of TE_{21} mode of $SWG_{\pi/2}$ is converted to TE_{11} for an upper and lower semi-circular aperture of the coaxial waveguide. Further, all power is converted to TE_{11} and *TEM* depending upon the orientation of the electric field. From Table 4.2, it can be concluded that the application of *Plate1* is worthful, and it prevents the formation of TE_{21} mode at port-F [Kumar *et al*. (2019)]. The SWG mode converter design having *Plate1* absent has analysed, whereas it requires impedance matching stubs as discussed in [Yuan *et al*. (2005)]. Thus, MMT developed in the present work is an important and useful tool to predict the content of the different modes present in its output and so to characterize the SWG mode converter performance.

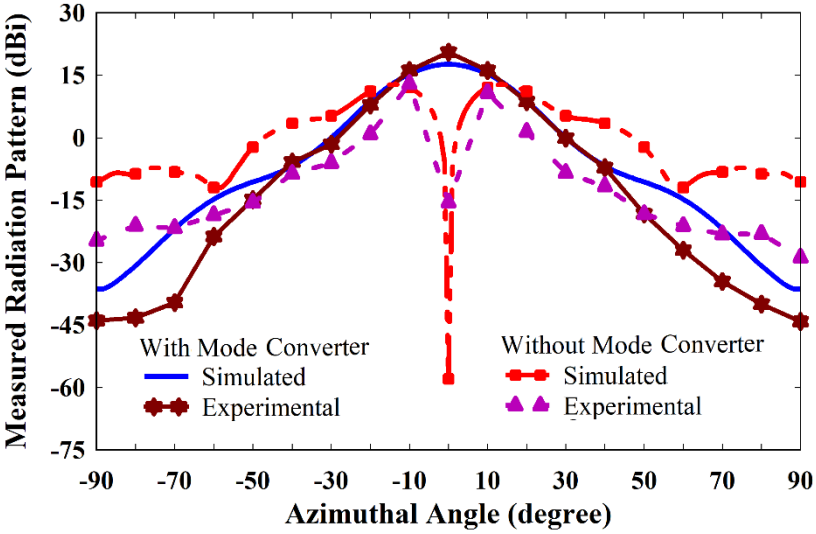

Figure 4.10. Comparison of conversion efficiency obtained from simulation between the input port-A to output port-G are compared with results obtained from the MMT analysis using input port-C to output port-G, are also compared with the measured result of Kumar *et al*. (2019).

Furthermore, the radiation pattern reported in (Kumar *et al*. 2019), as shown in Figure 4.9. The SWG mode converter structure reported in this paper is the same structure reported by Kumar *et al*. 2019, and their radiation pattern supports the conversion of TM_{01} to TE_{11}, as concluded by MMT. Computational modelling using MMT provides a faster analysis with more accuracy in comparison to CST. Also, in the future, further study has required some additional technique to visualize the combining of the field at port F.

4.4. Conclusions:

The sectoral waveguide (SWG) mode converters are linear, compact and efficient all-metal microwave device used to convert azimuthally symmetric *TEM* or TM_{01} modes to TE_{11} mode, which are often required for HPM systems. Generalized *N*-furcation network approach is used by separating the coaxial waveguide to SWGs and bifurcating SWG to SWG mode converter can be achieved. To evaluate the different electromagnetic modes and its content present in the output of the SWG mode converter, mode-matching analysis is used. A generalized formulation for evaluation of all the four scattering coefficients for all the modes is developed. The reflection and transmission scattering coefficients for the different modes computed through the developed analysis is found to be in agreement with those obtained using simulation codes. The proposed design is further investigated through simulation and mode matching analysis for the frequency range 2.8 GHz to 3.2 GHz. The mode conversion for TM_{01} mode to TE_{11} mode at frequency 3 GHz, of the proposed design, predicted conversion efficiency using mode-matching method ~99.1% and by the simulation ~98.6%. The work should be a useful and important tool for the electromagnetic characterization of the SWG mode converters and can easily be extended for another multi-junction device as well.